# Transient assembly of F-actin on the outer mitochondrial membrane contributes to mitochondrial fission

Sunan Li,[1,2] Shan Xu,[1,2] Brian A. Roelofs,[1,2] Liron Boyman,[1,3] W. Jonathan Lederer,[1,3] Hiromi Sesaki,[4] and Mariusz Karbowski[1,2]

[1]Center for Biomedical Engineering and Technology, [2]Department of Biochemistry and Molecular Biology, and [3]Department of Physiology, University of Maryland School of Medicine, Baltimore, MD 21201
[4]Department of Cell Biology, Johns Hopkins University School of Medicine, Baltimore, MD 21205

In addition to established membrane remodeling roles in various cellular locations, actin has recently emerged as a participant in mitochondrial fission. However, the underlying mechanisms of its participation remain largely unknown. We report that transient de novo F-actin assembly on the mitochondria occurs upon induction of mitochondrial fission and F-actin accumulates on the mitochondria without forming detectable submitochondrial foci. Impairing mitochondrial division through Drp1 knockout or inhibition prolonged the time of mitochondrial accumulation of F-actin and also led to abnormal mitochondrial accumulation of the actin regulatory factors cortactin, cofilin, and Arp2/3 complexes, suggesting that disassembly of mitochondrial F-actin depends on Drp1 activity. Furthermore, down-regulation of actin regulatory proteins led to elongation of mitochondria, associated with mitochondrial accumulation of Drp1. In addition, depletion of cortactin inhibited Mfn2 down-regulation– or FCCP-induced mitochondrial fragmentation. These data indicate that the dynamic assembly and disassembly of F-actin on the mitochondria participates in Drp1-mediated mitochondrial fission.

## Introduction

Balancing mitochondrial fusion and fission is necessary to maintain cellular homeostasis and adjust mitochondrial function to cellular needs. Disturbing this process causes mitochondrial dysfunction, ultimately leading to cellular demise (Youle and Karbowski, 2005; Chen et al., 2007; Knott et al., 2008; Benard and Karbowski, 2009; DuBoff et al., 2012; Nunnari and Suomalainen, 2012). Consistent with a critical role for mitochondrial dynamics in cell homeostasis, the wide spectrum of mitochondrial diseases, which typically concern deficiencies in the oxidative phosphorylation system (OXPHOS), now includes genetic and biochemical alterations of mitochondrial fusion and fission. For example, mutations in Mfn2 (mitochondrial fusion factor Mitofusin 2) result in CMT2A (Charcot-Marie-Tooth Neuropathy type 2A; Züchner et al., 2004), an inherited disorder of the peripheral nervous system. Mutations in the inner mitochondrial membrane (IMM) protein Opa1 (Optic Atrophy 1) cause autosomal dominant optic atrophy (DOA; Alexander et al., 2000).

Mitochondrial division is a multistep process relying on the action of several proteins. Control of the essential mitochondrial fission protein Drp1 (Dynamin-related protein 1) appears to be the primary function of these proteins (Bui and Shaw, 2013; Losón et al., 2013). The recruitment of Drp1 from the cytosol to the outer mitochondrial membrane (OMM) is mediated by integral OMM-associated Drp1 receptors, mitochondrial fission factor (Mff; Gandre-Babbe and van der Bliek, 2008; Otera et al., 2010), mitochondrial division proteins 49 and 51 (MiD49/51; Palmer et al., 2011), and Fis1 (Yoon et al., 2003; Losón et al., 2013). Specific roles of other Mffs, including SUMO proteases SENP3 and SENP5 (Zunino et al., 2009; Guo et al., 2013), and ubiquitin E3 ligase MARCH5 (Karbowski et al., 2007) in relation to Drp1 recruitment are not clear. However, upon recruitment to the mitochondria Drp1 forms homo and

Correspondence to Mariusz Karbowski: mkarbowski@umaryland.edu

Abbreviations used in this paper: AvDev, average deviation; IMM, inner mitochondrial membrane; MEF, mouse embryonic fibroblast; Mff, mitochondrial fission factor; mito-PAGFP, mitochondrial matrix–targeted photoactivatable GFP; OMM, outer mitochondrial membrane.



The Rockefeller University Press $30.00
J. Cell Biol. Vol. 208 No. 1 109–123
www.jcb.org/cgi/doi/10.1083/jcb.201404050

hetero oligomers. These form spirals around constricted sites on mitochondria in the final steps of mitochondrial fission that mediate membrane scission (Ingerman et al., 2005; Bui and Shaw, 2013). This process appears to be facilitated by ER tubules that colocalize with mitochondrial fission sites (Friedman et al., 2011; Korobova et al., 2013; Stavru et al., 2013). Subsequently, disassembly and translocation of Drp1 from the mitochondria to the cytosol completes the mitochondrial fission pathway. It is likely that mitochondrial fission steps downstream of mitochondrial recruitment of Drp1 are regulated by some of the above-mentioned accessory proteins. Consistent with this notion, SENP3 and SENP5, as well as MARCH5, were proposed to regulate Drp1 trafficking between the cytosol and mitochondria (Karbowski et al., 2007; Zunino et al., 2007; Guo et al., 2013).

Recent evidence supports a role for the actin cytoskeleton in mitochondrial division. For example, although pharmacological inhibition of F-actin polymerization did not affect mitochondrial structure, it attenuated mitochondrial toxin-induced mitochondrial fragmentation (De Vos et al., 2005). Other reports showed that treatment with actin polymerization inhibitor latrunculin B (LatB) led to mitochondrial elongation in otherwise untreated U2OS osteosarcoma cells (Korobova et al., 2013) but decreased mitochondrial size in cultured neurons (Beck et al., 2012). These findings suggest that F-actin may regulate mitochondrial size perhaps through recruitment to or retention of Drp1 on the mitochondria.

Consistent with this notion, in a *Drosophila* model of tauopathy, excess tau-induced F-actin stabilization inhibited association of Drp1 with mitochondria, leading to mitochondrial elongation and subsequent neurotoxicity (DuBoff et al., 2012). Conversely, in mammalian cells, inhibition of actin polymerization or down-regulation of the ER-localized actin binding protein INF2 (inverted formin 2) reduced mitochondrial association of Drp1 (De Vos et al., 2005; Korobova et al., 2013). Considering these reports, it is possible that it is not the status of actin (polymerized versus monomeric) but rather dynamic remodeling of the actin cytoskeleton on the mitochondria that regulates mitochondrial association of Drp1 and potentially Drp1-driven mitochondrial fission. Because overexpression of MiD49/51, mitochondrial receptors of Drp1, led to mitochondrial elongation that was associated with abnormal mitochondrial accumulation of F-actin, it is also possible that mitochondrial fission proteins might be implicated in mitochondrial assembly of F-actin (Palmer et al., 2011). Actin depolymerization by cytochalasin D reduced Drp1-independent mitochondrial division induced by pore-forming toxin listeriolysin (LLO; Stavru et al., 2013), indicating that F-actin may also contribute to non–Drp1-related mechanisms of mitochondrial fission. Despite the many lines of evidence pointing to a role for actin in regulating mitochondrial morphology, the mechanism remains unclear.

Here, we report that transient Drp1-independent de novo polymerization of F-actin on the OMM contributes to mitochondrial division in mammalian cells. We also found that mitochondrial division and mitochondrial assembly of F-actin were controlled by the actin regulatory proteins cortactin, cofilin, and Arp2/3 complexes.

## Results

### Accumulation of F-actin on the mitochondria in Drp1$^{-/-}$ mouse embryonic fibroblasts (MEFs)

Accumulating evidence suggests a role for the actin cytoskeleton in both Drp1-dependent and Drp1-independent mitochondrial division (De Vos et al., 2005; DuBoff et al., 2012; Korobova et al., 2013; Stavru et al., 2013). However, the mechanism and the scope of cross talk between mitochondrial fission and actin are not well defined. We analyzed the spatial relation between F-actin and mitochondria in wild-type MEFs and in Drp1$^{-/-}$ MEFs (Fig. 1, A–E). To detect F-actin, cells were labeled with Alexa Fluor 546 phalloidin (Alexa-phalloidin), a high-affinity F-actin probe. Mitochondria were immunolabeled with anti–cytochrome *c* antibody, followed by structured illumination imaging. Although specific colocalization between F-actin and mitochondria was not detectable in untreated wild-type MEFs (Fig. 1, A and E), Alexa-phalloidin colocalized with mitochondria in ∼20% of Drp1$^{-/-}$ MEFs (20.2 ± 4.1%; Fig. 1, C and E). This colocalization was primarily restricted to the perinuclear mitochondria (Fig. 1 C). Confirming the specificity of F-actin colocalization with mitochondria in Drp1$^{-/-}$ MEFs, mitochondrial F-actin was not detected in Mfn2$^{-/-}$ MEFs (Fig. 1 E), and only 5.7 ± 4.6% HeLa cells displayed some F-actin colocalization with mitochondria (Fig. 1 E). However, F-actin was also found to colocalize in ∼34% of mitochondrial Drp1 receptor Mff knockout (Mff$^{-/-}$) cells (34.4 ± 3.0%; Figs. 1 E and S1). Thus, inhibition of mitochondrial fission either by loss of Drp1 or reduction of Drp1 interaction with mitochondria resulted in abnormal mitochondrial accumulation of F-actin.

### Transient de novo polymerization of F-actin on the mitochondria upon stress-induced mitochondrial fission

Transient F-actin assembly has been implicated in various membrane remodeling events including dynamin-dependent endocytosis (Mooren et al., 2012). Furthermore, knockout of dynamin, a large GTPase essential for endocytotic vesicle scission led to abnormal accumulation of F-actin at the defective vesicle scission sites (Ferguson et al., 2009). A similar scenario may also underlie mitochondrial accumulation of F-actin in mitochondrial fission deficient Drp1$^{-/-}$ and Mff$^{-/-}$ MEFs.

To verify this possibility, we tested the degree to which F-actin assembles on mitochondria upon stress-induced mitochondrial fission. Drp1-mediated mitochondrial fission can be induced by mitochondrial toxins, including the uncoupling agents carbonyl cyanide 4-(trifluoromethoxy) phenylhydrazone (FCCP) and 2-[2-(3-Chlorophenyl) hydrazinylyidene] propanedinitrile (CCCP; Cereghetti et al., 2008; Gandre-Babbe and van der Bliek, 2008; Palmer et al., 2011; Stavru et al., 2013). Wild-type MEFs and Drp1$^{-/-}$ MEFs were treated with FCCP as indicated in Fig. 1 E, followed by immunofluorescence to detect F-actin using Alexa-phalloidin and mitochondria using anti–cytochrome *c* antibody (Fig. 1, B, D, and E). The data showed increase in several cells with F-actin–positive mitochondria in FCCP wild-type and Drp1$^{-/-}$ MEFs peaking at 2–5 min of treatment, followed by

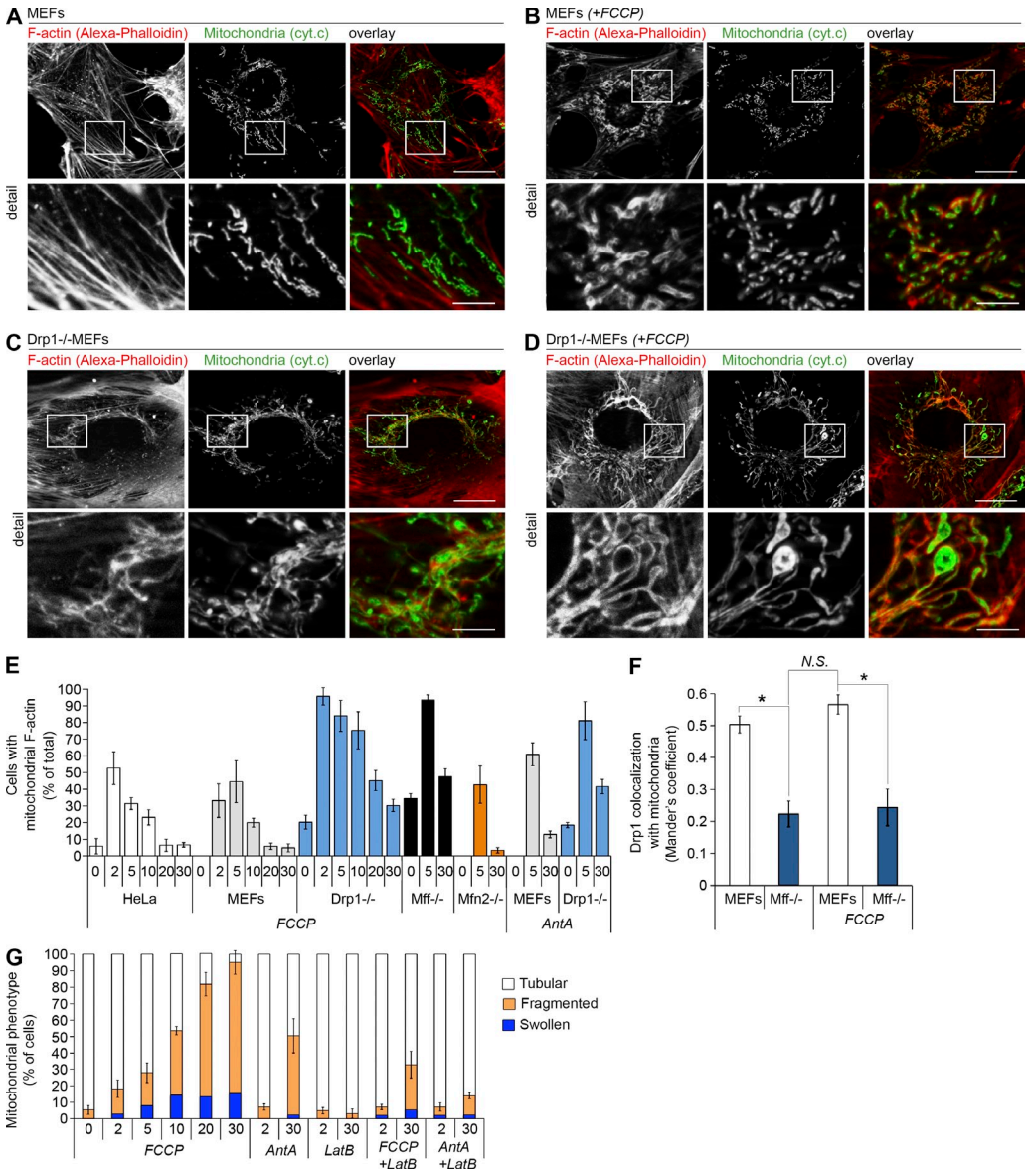


Figure 1. **Localization of F-actin on the mitochondria.** (A–D) Wild type (A and B) and Drp1$^{-/-}$ (C and D) MEFs were treated with FCCP (B and D) or DMSO (A and C) for 2 min, and then labeled with Alexa-phalloidin to detect F-actin (red) and immunostained with anti–cytochrome *c* mAb (green) to detect mitochondria. Bars: 20 µm; (detail) 5 µm. The mitochondria-enriched z-sections corresponding to the vertical middle part of the cells are shown here and thereafter. These images largely lack the cortical F-actin signal, which is detectable in the bottom of the cells, corresponding to z-sections below those enriched in the mitochondria. The typical z-stacks are shown in Fig. S2. These z-stack series also reveal the relative intensity of mitochondria-associated F-actin versus cortical F-actin. (E) Quantification of the number of cells showing mitochondrial accumulation of F-actin. Wild-type, Drp1$^{-/-}$, Mff$^{-/-}$, and Mfn2$^{-/-}$ MEFs, as well as HeLa cells, were treated with FCCP or AntA as indicated in the figure followed by immunofluorescence and cell counting. Means ± average deviation (AvDev) of triplicate counting of 150 cells/condition are shown. (F) Colocalization of Drp1 with mitochondria was analyzed in wild-type and Mff$^{-/-}$ MEFs. The values represent Mander's correlation coefficient (Rr) that reveal the degree of association of pixels in different channels of the image. Data represent the mean ± SD of 15 images/condition. Each image used for the analysis contained at least two cells. *, P < 0.001. (G) Quantification of the number of cells with different mitochondrial phenotypes in FCCP- AntA-, LatB-, LatB+FCCP-, and LatB+AntA-treated wild-type MEFs. Typical examples of cells and specific mitochondrial phenotypes are shown in Fig. S3. Means ± AvDev from a representative experiment after triplicate counting of 150 cells/condition are shown.

a gradual decline in the number of cells with F-actin–positive mitochondria (Fig.1, D and E). However, there was a major difference in the number of cells with F-actin–positive mitochondria between wild-type and Drp1$^{-/-}$ MEFs. At 2 min into FCCP treatment, ~100% of Drp1$^{-/-}$ MEFs displayed a clear mitochondrial accumulation of F-actin, in contrast to ~33% in the case of wild-type MEFs (Figs. 1 E and S1). Similar mitochondrial accumulation of F-actin at 2 min of FCCP treatment was also detected in ~100% of Mff$^{-/-}$ MEFs (Figs. 1 E and S1). Furthermore, parallel analyses of Mfn2$^{-/-}$ MEFs and HeLa cells revealed transient increases in the number of cells with F-actin–positive mitochondria occurring at comparable rates as FCCP-treated wild-type MEFs (Figs. 1 E and S1). Treatment with the cytochrome *c* reductase inhibitor Antimycin A (AntA), another inducer of mitochondrial division (De Vos et al., 2005), also led to mitochondrial accumulation of F-actin (Figs. 1 E and S1). As with FCCP treatment, mitochondrial accumulation of F-actin was more pronounced in AntA-treated Drp1$^{-/-}$ MEFs

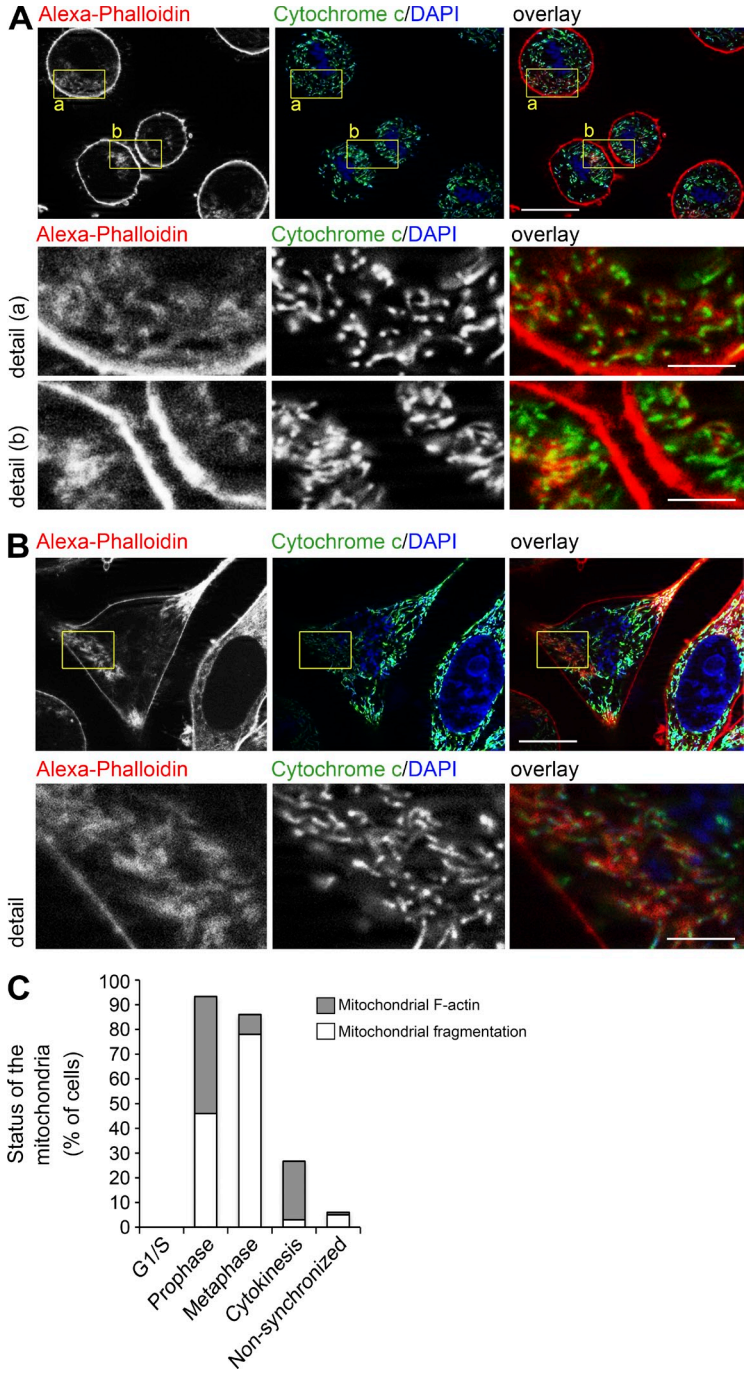


Figure 2. **Spatial relation of F-actin and mitochondria in mitotic cells.** (A and B) HeLa cells were synchronized in $G_1$/S phase of the cell cycle using a double thymidine block procedure and subsequently released into thymidine-free medium to restart the cell cycle progression. Cells were fixed at 8.5 h after release and stained with anti–cytochrome *c* mAbs (A and B overlay images; green; to reveal mitochondria), Alexa-phalloidin (A and B overlay images; red, to reveal F-actin), and DAPI (A and B overlay images, blue; to reveal DNA), followed by structured illumination imaging. The examples of anaphase (A) and prophase (B) cells that were identified based on the chromosomal status and distribution are shown. Higher magnification of insets marked with yellow rectangles in A and B are shown in detail images. Bars: 20 µm; (detail) 5 µm. (C) Cells in different stages of mitosis were analyzed for mitochondrial assembly of F-actin and mitochondrial morphology. Data represent quantification of ∼70 cells per mitotic stage.

than AntA-treated wild-type MEFs (Fig. 1 E). We also tested mitochondrial colocalization of Drp1 in control and FCCP-treated wild-type MEFs and Mff$^{-/-}$ MEFs (Fig. 1 F). As expected (Otera et al., 2010), Mff ablation significantly reduced mitochondrial localization of Drp1. Furthermore, there was only a minor increase in mitochondrial Drp1 in FCCP-treated cells. Thus, mitochondrial accumulation of F-actin appears to preferentially occur in cells in which Drp1 fission complex formation is inhibited, and may occur before Drp1 activation in control cells.

We tested whether mitochondrial accumulation of F-actin requires de novo actin polymerization. Cells were pretreated with LatB, an actin polymerization inhibitor, for 2 min, followed by treatment with either FCCP for 2 or 10 min or AntA for 5 or 10 min. Because there was no detectable mitochondrial F-actin accumulation in LatB-pretreated FCCP- or AntA-treated wild-type and Drp1$^{-/-}$ MEFs (unpublished data), we conclude that de novo actin polymerization is required for mitochondrial accumulation of F-actin.

The effect of LatB on mitochondrial structure was also tested (Figs. 1 G and S3). Wild-type MEFs were treated with FCCP, AntA, or LatB, or were pretreated with LatB followed by FCCP or AntA, as indicated (Fig. 1 G). Although there was no clear difference in mitochondrial structure between untreated and LatB-treated cells, LatB pretreatment decreased FCCP- and AntA-induced mitochondrial fragmentation (Figs. 1 G and S3). Confirming earlier reports (De Vos et al., 2005; Cereghetti et al.,

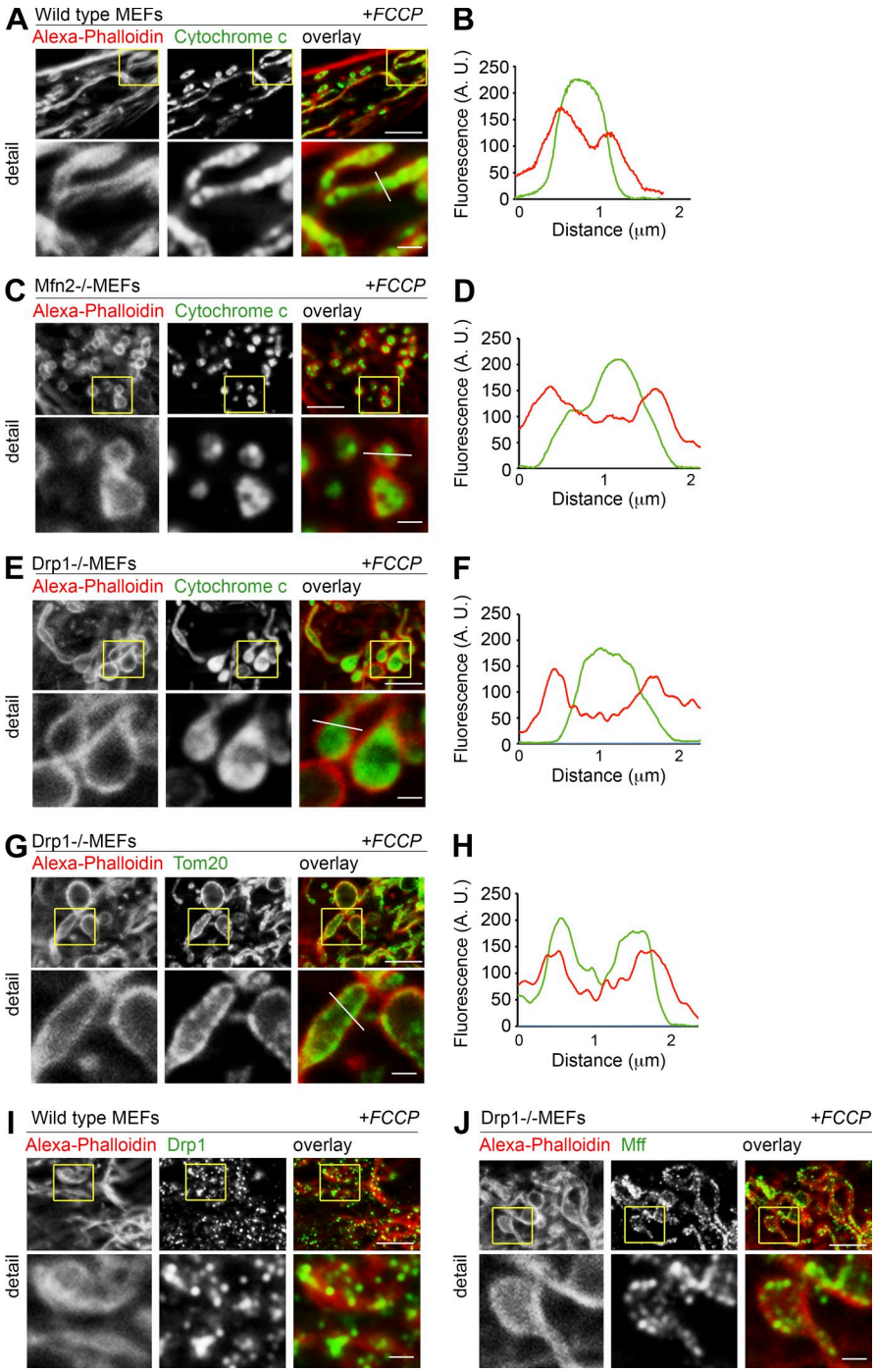


Figure 3. **Submitochondrial distribution of F-actin in FCCP-treated cells.** Wild-type (A and I), Mfn2$^{-/-}$ (C), and Drp1$^{-/-}$ (E, G, and J) MEFs were treated with FCCP for 2 min, followed by immunofluorescence. High magnification structured illumination images of Alexa-phalloidin (A, C, E, G, I, and J)–labeled mitochondria-associated F-actin are shown. Mitochondrial inner membrane and intermembrane space were revealed by cytochrome *c* (A, C, and E), the OMM was revealed by immunoblotting for Tom20 (G) and Mff (J), and the OMM-associated Drp1 was detected with anti-Drp1 mAb (I). Bars: 5 µm; (detail) 1 µm. Fluorescence linescans along the lines shown in the respective detail panels are also shown (B, D, F, and H). Similar linescan patterns were obtained in several ($n$ > 10) independent immunofluorescence experiments.

2008; Gandre-Babbe and van der Bliek, 2008), FCCP and AntA did not significantly affect mitochondrial structure in Drp1$^{-/-}$ MEFs, except for some mitochondrial swelling (unpublished data).

### Mitochondrial assembly of F-actin in mitotic cells

Interconnected mitochondrial networks become fragmented in mitotic cells in a Drp1-dependent manner (Taguchi et al., 2007; Zunino et al., 2009; Kashatus et al., 2011), probably facilitating stochastic mitochondrial segregation into two daughter cells. To test whether mitochondrial accumulation of F-actin also occurs during mitosis, cells were synchronized in the $G_1$/S phase of the cell cycle using a double thymidine block procedure and subsequently released into thymidine-free medium to restart cell cycle progression. Cells were fixed at different time points after release up to 10 h and stained with Alexa-phalloidin, anti–cytochrome *c* antibody, and DAPI to detect DNA, followed by structured illumination imaging. Because accumulation of mitotic cells was most pronounced at 8–9 h after release (not depicted), cells fixed at 8.5 h after release were analyzed (Fig. 2). The data showed that in mitotic cells mitochondria were aligned along the F-actin cytoskeleton (Fig. 2, A and B). Although mitochondrial fragmentation was apparent in ∼80% of anaphase cells and ∼85% of these cells showed mitochondrial association of

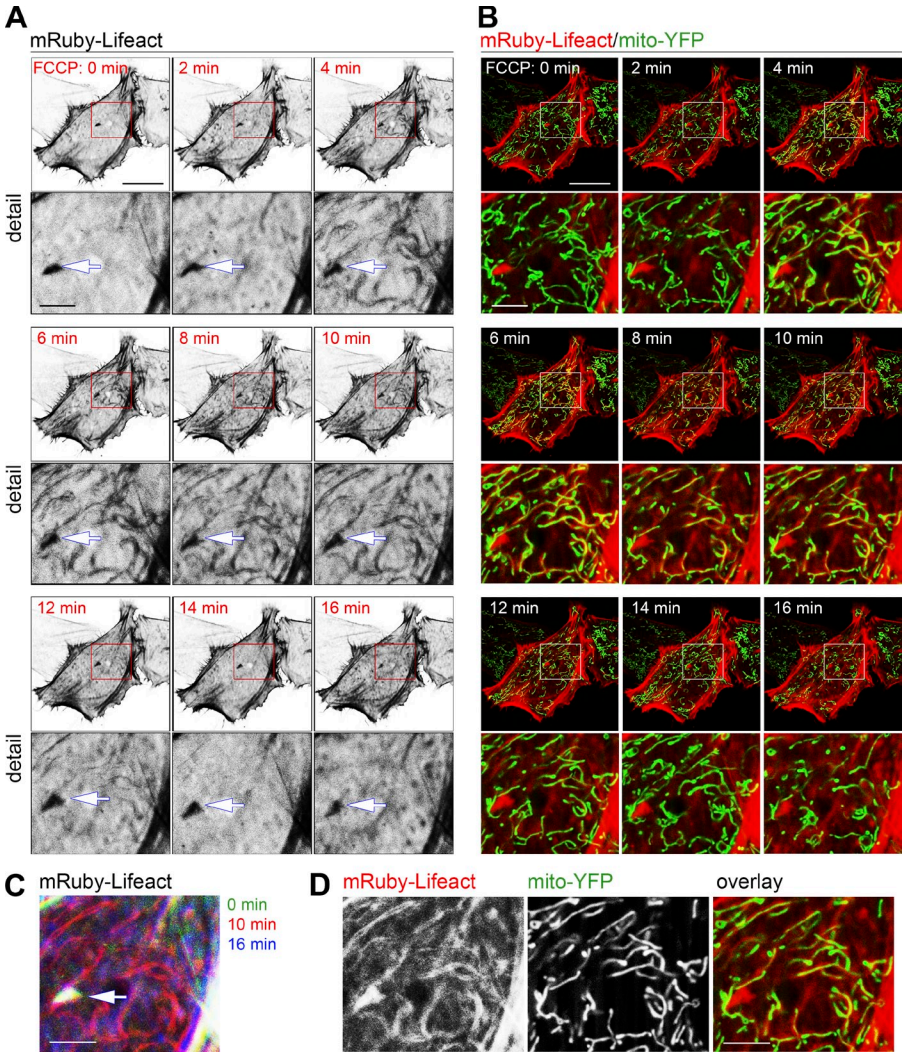


Figure 4. **Mitochondrial assembly of F-actin in living cells.** (A and B) HeLa cells expressing mRuby-Lifeact (red in B) and mito-YFP (green in B) were treated with FCCP as indicated, followed by a time-lapse structural illumination imaging. In A, fluorescence images of mRuby-Lifeact are shown. To enable easier interpretation of the data, fluorescent images were inverted. Bars: 20 µm; (detail) 5 µm. (C) Pseudocolored images showing the mitochondrial F-actin assembly at 0 min (green), 10 min (red), and 16 min (blue) after addition of FCCP within the red rectangle shown in A. Note a dominant red signal in C indicating a high level of mitochondrial F-actin at 10 min of FCCP treatment, as compared with 0 min and 16 min. Arrows in A and C indicate F-actin–positive structures that are not altered by FCCP treatment, which shows a white pseudocolored signal in C. (D) Details from marked area in the image taken at 10 min (shown in A) of FCCP treatment. Bars, 5 µm.

F-actin (Fig. 2, A–C), mitochondrial assembly of F-actin was also detectable in ∼95% of prophase cells, ∼45% of which displayed mitochondrial fragmentation (Fig. 2, B and C). Thus, it appears that in a similar manner as in stress-induced mitochondrial fission, mitochondrial assembly of F-actin also precedes mitochondrial division in mitotic cells.

### F-actin accumulates on the OMM without forming submitochondrial foci

Analyses of FCCP-treated wild-type, Drp1$^{-/-}$, and Mfn2$^{-/-}$ MEFs (Fig. 3) and similarly treated HeLa cells (Fig. S1) revealed that F-actin did not colocalize with the cytochrome *c*–positive IMM, intermembrane space, or mitochondrial cristae but rather formed cytochrome *c* circumscribing rings (Fig. 3, A–F), consistent with OMM localization. Indeed, in FCCP-treated cells Alexa-phalloidin colocalized with Tom20, a marker of the OMM (Fig. 3, G and H). Furthermore, the Alexa-phalloidin signal was equally distributed with no apparent colocalization with Drp1 (Fig. 3 I). Because Drp1 colocalizes with submitochondrial foci formed by Mff, a mitochondrial receptor of Drp1 (Otera et al., 2010), we also tested the degree to which Mff colocalized with mitochondrial F-actin in Drp1$^{-/-}$ MEFs. Although there was a clear overlap between Alexa-phalloidin and Mff, we did not detect any accumulation of F-actin on the punctate OMM-associated foci formed by Mff (Fig. 3 J).

### Mitochondrial accumulation of F-actin in living cells

To verify mitochondrial assembly of F-actin independently, we applied a red fluorescent protein mRuby-tagged Lifeact (mRuby-Lifeact). Lifeact is a 17–aa peptide derived from the N-terminal domain of actin binding protein 140 (Abp140) (Riedl et al., 2008). It has been shown that fluorescent-tagged Lifeact interacts with F-actin with ∼30× greater affinity than with G-actin, enabling visualization of local F-actin polymerization associated with various cellular pathways (Riedl et al., 2008, 2010; Taylor et al., 2011). Another benefit of mRuby-Lifeact is its applicability to live cell imaging.

Cells were cotransfected with mRuby-Lifeact and mito-YFP followed by time-lapse microscopy. Although the use of wide field fluorescence imaging failed to detect mitochondria-associated mRuby-Lifeact in a clear manner (not depicted), application of a structured illumination imaging method reduced background and cortical F-actin–derived fluorescence, enabling unambiguous visualization of FCCP-induced dynamic changes of F-actin on the mitochondria (Figs. 4 and S4). The data

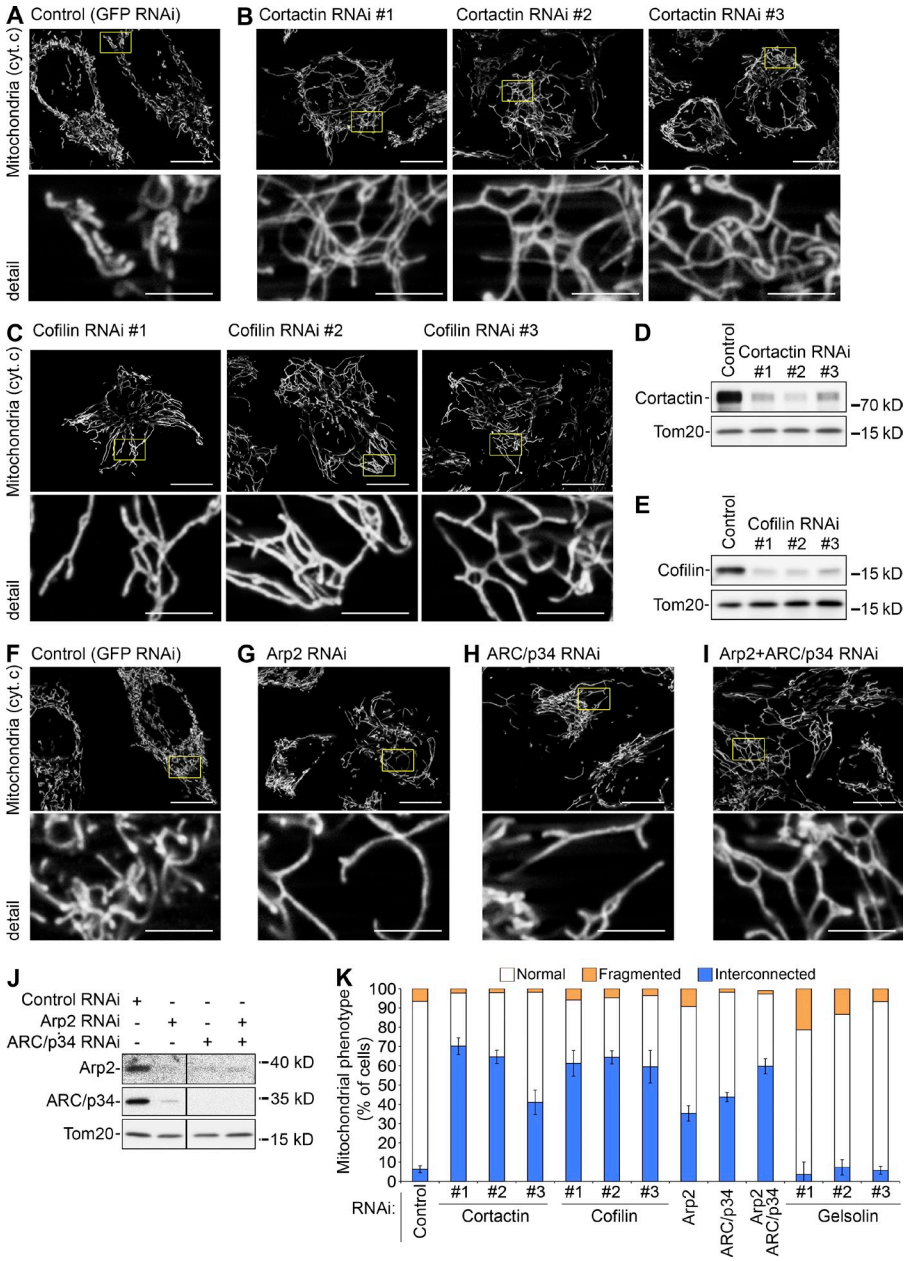


Figure 5. **Down-regulation of cortactin, cofilin, and components of the Arp2/3 complex result in abnormal mitochondrial elongation/interconnection.** (A–J) Control RNAi (A and F), cortactin RNAi cells (obtained using three distinct cortactin RNAi constructs; B), cofilin RNAi cells (obtained using three distinct cofilin RNAi constructs; C), Arp2 RNAi cells (achieved with a mix of two independent Arp2 targeting RNAi constructs; G), ARC/p34 RNAi cells (achieved with a mix of two independent ARC/p34 targeting RNAi constructs; H), and combined double Arp2 and ARC/p34 RNAi cells (achieved with one RNAi construct per each target; I) were immunostained with anti–cytochrome *c* mAb to reveal mitochondria, followed by structured illumination imaging. Higher magnifications of areas marked with yellow rectangles are shown in detail images. Bars: 20 µm; (detail) 5 µm. Down-regulation levels of cortactin (D), cofilin (E), and Arp2 and ARC/p34 (J) were analyzed by Western blotting in total cell lysates obtained from respective RNAi cells. Tom20 was used as a loading control. (K) Mitochondrial morphology in control RNAi, cortactin RNAi (constructs #1–3), cofilin RNAi (constructs #1–3), and Arp2/p34 RNAi cells were quantified as indicated in the figure. Data represent mean ± AvDev from a representative experiment after triplicate counting of 150 cells/condition. Values for the control RNAi cells were obtained by averaging two triplicate counts of 150 cells/condition obtained independently in cortactin/cofilin and Arp2/p34 RNAi experiments. Mitochondrial morphology in gelsolin RNAi cells was also quantified in a similar manner.

showed mitochondrial accumulation of mRuby-Lifeact starting at ∼4 min (Fig. 4, A and B), with a gradual decline in mitochondrial levels of mRuby-Lifeact at ∼12 min after initial detection (Fig. 4, A–C). Importantly, the diffused OMM localization pattern of mRuby-Lifeact (Fig. 4, B and D) was reminiscent of that observed in Alexa-phalloidin–labeled fixed cells (Figs. 1 and 3). This was also apparent in cells expressing Drp1$^{K38A}$, a dominant-negative mutant of Drp1 (Fig. S4). Further confirming the Alexa-phalloidin labeling results in Drp1$^{-/-}$ MEFs (Fig. 1), the data also showed accumulation of F-actin on the perinuclear mitochondria in untreated Drp1$^{K38A}$-expressing HeLa cells but not in wild-type Drp1-overexpressing HeLa cells (Fig. S4). Furthermore, pretreatment with LatB for 2 min before FCCP application also inhibited mitochondrial accumulation of mRuby-Lifeact in control and Drp1$^{K38A}$-expressing cells (unpublished data).

The calponin homology domain of utrophin (mCherry-UtrCH), another live cell actin probe (Burkel et al., 2007), was also applied to further verify mitochondrial assembly of F-actin. Cells cotransfected with mCherry-UtrCH and mito-YFP were treated with FCCP followed by time-lapse imaging. Like mRuby-Lifeact, mCherry-UtrCH accumulated on the mitochondria in FCCP-treated cells (Fig. S5). This accumulation was also transient and occurred in a similar time frame as accumulation of mRuby-Lifeact.

## Down-regulation of cortactin, cofilin, or Arp2/3 complexes results in abnormal interconnection and elongation of mitochondria

Based on the data discussed above and the fact that activity of INF2 (inverted formin 2), which is already linked to Drp1-mediated

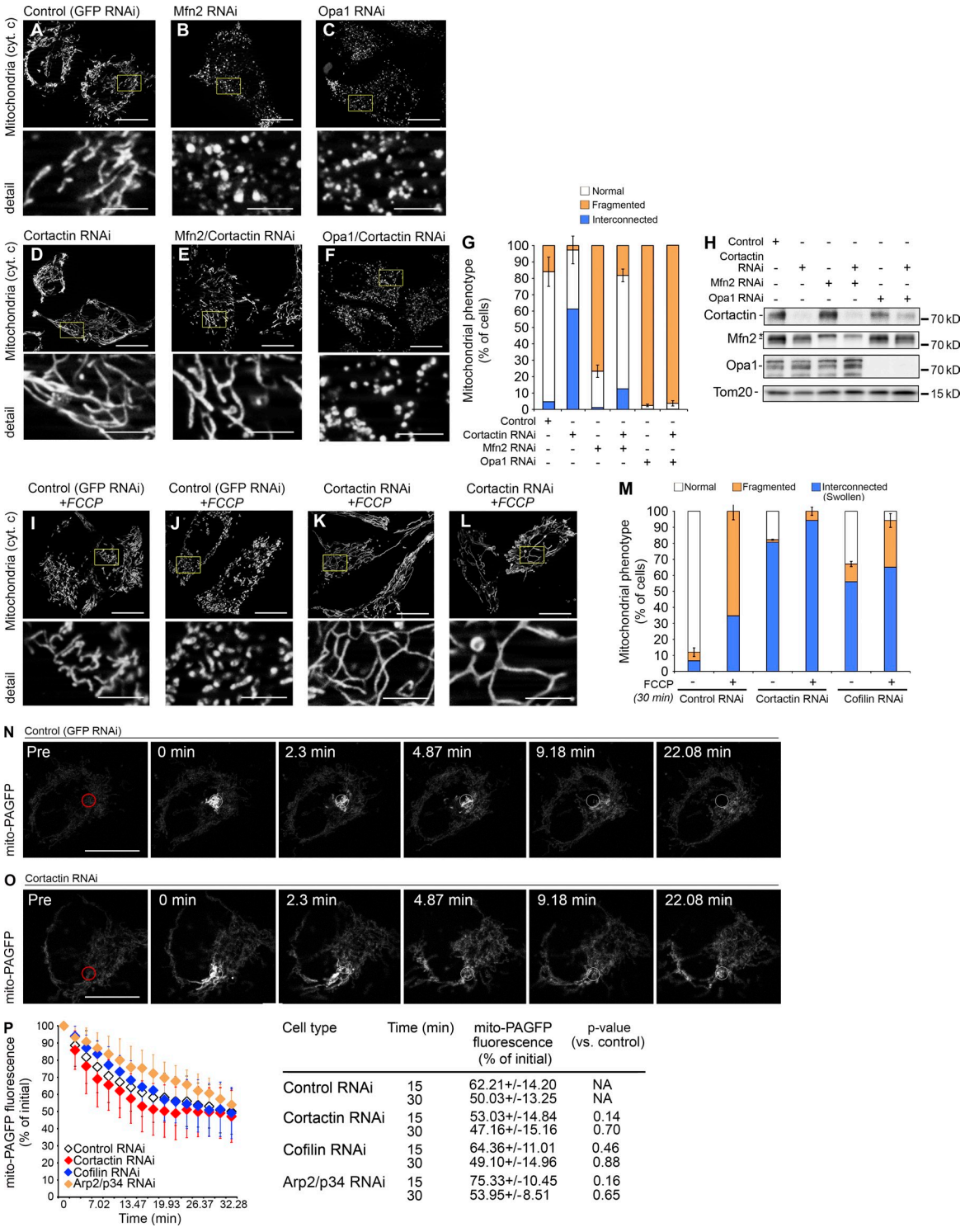


| Cell type | Time (min) | mito-PAGFP fluorescence (% of initial) | p-value (vs. control) |
|---|---|---|---|
| Control RNAi | 15 | 62.21+/-14.20 | NA |
| | 30 | 50.03+/-13.25 | NA |
| Cortactin RNAi | 15 | 53.03+/-14.84 | 0.14 |
| | 30 | 47.16+/-15.16 | 0.70 |
| Cofilin RNAi | 15 | 64.36+/-11.01 | 0.46 |
| | 30 | 49.10+/-14.96 | 0.88 |
| Arp2/p34 RNAi | 15 | 75.33+/-10.45 | 0.16 |
| | 30 | 53.95+/-8.51 | 0.65 |

Figure 6. **Cortactin, cofilin, and Arp2 complexes control mitochondrial division.** (A–F) Control RNAi (A, I, and J), Mfn2 RNAi (B), Opa1 RNAi (C), cortactin RNAi (construct #1; D, K, and L) cells, as well as double Mfn2/cortactin RNAi (E) and double Opa1/cortactin RNAi cells (F), were immunostained with anti–cytochrome *c* mAb to reveal mitochondria, followed by structured illumination imaging. Higher magnifications of areas marked with yellow rectangles are shown in detail images. Bars: 20 µm; (detail) 5 µm. (G) Mitochondrial morphologies in cells described above (A–F) were quantified as indicated in the figure. Data represent mean ± AvDev from a representative experiment after triplicate counting of 150 cells/condition. (H) Protein levels in cells described above (A–F) were analyzed by Western blotting in total cell lysates. Tom20 was used as a loading control. The asterisk indicates an x-reactive protein detectable with anti-Mfn2 antibody. Control RNAi (I and J) and cortactin RNAi (construct#1; K and L) treated with either DMSO (vehicle; I and K) or FCCP (J and L) for 30 min and immunostained with anti–cytochrome *c* mAb are shown. Bars: 20 µm; (detail) 5 µm. (M) Mitochondrial morphologies in vehicle- and FCCP-treated control RNAi, cortactin RNAi (#1), and cofilin RNAi (#1) cells were quantified as indicated in the figure. Data represent mean ± AvDev from a representative experiment after triplicate counting of 150 cells/condition. (N–P) Mitochondrial fusion rates in control (N and P), cortactin (O and P), cofilin (P), and Arp2 (P) RNAi cells were analyzed using mito-PAGFP–based mitochondrial fusion assay (Karbowski et al., 2004, 2006). In N and O, typical images from a time-lapse series of control (N) and cortactin RNAi (O) cells are shown. Bars, 20 µm. In P, mito-PAGFP fluorescence changes in control, cortactin, cofilin,

mitochondrial fission (Korobova et al., 2013), did not appear to mediate mitochondrial accumulation of F-actin similar to what we demonstrated here (Figs. 1–4), we sought to determine whether proteins other than INF2 actin-modifying proteins could also regulate mitochondrial fission. We analyzed the degree to which overexpression or down-regulation of WASp, cortactin, Arp2/3 complex, formin1, FBNP17 (formin-binding protein 17), gelsolin, cofilin, Abp1, or coronin affect mitochondrial network organization. This selection was based on the established role for each of these factors in the regulation of the actin cytoskeleton in membrane remodeling in non-mitochondrial compartments, including clathrin-dependent and -independent endocytosis (Taylor et al., 2011; Mooren et al., 2012; Salbreux et al., 2012; Stoeber et al., 2012; Bravo-Cordero et al., 2013; Blanchoin et al., 2014). Although overexpression of any of the above-mentioned proteins did not affect mitochondrial network organization (not depicted), down-regulation of cortactin (Fig. 5, B, D, and K) and cofilin (Fig. 5, C, E, and K) led to dramatic elongation and interconnection of mitochondria, as compared with control RNAi cells (Fig. 5, A and K). Because consistent mitochondrial alterations were apparent in cells transfected with three independent shRNAi vectors targeting cortactin (Fig. 5, B and D) or cofilin (Fig. 5, C and E), these effects are likely specific. Furthermore, separate or combined down-regulation of critical components of F-actin nucleation initiator Arp2/3 complex, Arp2, or ARC/p34 also led to an increase in the number of cells with elongated mitochondria (Fig. 5, G–I and K). Interestingly, down-regulation of ARC/p34 occurred in Arp2 RNAi cells, and depletion of Arp2 was seen in ARC/p34 RNAi cells (Fig. 5 J). These data suggest the possibility that depletion of a single component of Arp2/3 complex destabilizes the other components of this complex.

### Down-regulation of actin regulatory proteins inhibits Mfn2 down-regulation– or FCCP-induced mitochondrial fragmentation

We also found that down-regulation of cortactin restored tubular mitochondria in mitochondrial fusion factor Mitofusin 2–depleted cells (Mfn2 RNAi; Fig. 6, E and G). Specifically, although down-regulation of Mfn2 alone led to formation of fragmented mitochondrial networks in 76.7 ± 3.9% of the cells (Fig. 6, B and G), cortactin/Mfn2 double RNAi displayed mitochondrial fragmentation in only 18.2 ± 3.8% of cells (Fig. 6, E and G). Furthermore, there was no detectable effect of cortactin RNAi on mitochondria fragmentation induced by down-regulation of Opa1 (Fig. 6, C, F, and G). Considering that Mfn2 depletion results in partial inhibition of mitochondrial fusion, although Opa1 down-regulation leads to complete fusion inhibition, it is likely that restoration of mitochondrial tubules observed in cortactin/Mfn2 double RNAi cells is due to Mfn1-dependent mitochondrial fusion activity. We also tested the role of cortactin and cofilin in FCCP-induced mitochondrial division. To this end, FCCP-treated (Fig. 6, J, L, and M) or untreated Fig. 6, I, K, and M) control RNAi (Fig. 6, I, J, and M), cortactin RNAi (Fig. 6, K, L, and M), and cofilin RNAi (Fig. 6 M) cells were stained with anti–cytochrome *c* antibody followed by analysis of mitochondrial morphology. Supporting the role of cortactin and cofilin in mitochondrial division, down-regulation of either of these proteins inhibited FCCP-induced mitochondrial fragmentation (Fig. 6 M).

### Down-regulation of actin regulatory proteins does not affect mitochondrial fusion rates

Under certain situations, mitochondrial elongation and interconnection are induced not by inhibition of mitochondrial division but rather through the activation of mitochondrial fusion in a process called SIMH (stress-induced mitochondrial hyperfusion; Tondera et al., 2009). To test the effects of cortactin, cofilin, and Arp2/3 complex down-regulation on mitochondrial fusion rates, we applied a mitochondrial matrix–targeted photoactivatable GFP (mito-PAGFP)–based mitochondrial fusion assay (Karbowski et al., 2004, 2006; Tondera et al., 2009). Regions of interest (red circles in preactivation; "Pre" images in Fig. 6, N and O) in mito-PAGFP–expressing control, cortactin, cofilin, and Arp2+ARC/p34 RNAi cells were photoactivated by brief irradiation with UV light, followed by time-lapse imaging with 488-nm light every ∼2 min, over ∼30 min (Fig. 6, N–P). Quantification of mito-PAGFP fluorescence changes (Karbowski et al., 2004, 2006) in several time-lapse experiments revealed similar fusion rates in all analyzed cell groups (Fig. 6 P). The efficient protein down-regulation in each experiment was verified by Western blotting (unpublished data). These data further support the possibility that it is not induction of mitochondrial fusion but rather inhibition of mitochondrial fission that induces the mitochondrial elongation and interconnection observed in cortactin, cofilin, and the Arp2/3 complex RNAi cells.

### Down-regulation of cortactin or cofilin induces mitochondrial accumulation of Drp1

To gain insight into the mechanism by which cortactin and cofilin regulate mitochondrial division, we analyzed the mitochondrial localization of Drp1. Control RNAi (Fig. 7, A and D), cortactin RNAi (Fig. 7, B and D), and cofilin RNAi (Fig. 7, C and D) cells were immunostained for Drp1 and Tom20 to reveal the OMM, followed by structured illumination imaging (Fig. 7, A–C). Surprisingly, we found that down-regulation of both cortactin and cofilin led to significant increases in the amount of mitochondria-associated Drp1 (Fig. 7, B–D). The degree of colocalization of Tom20-labeled mitochondria and Drp1 was quantified and reported as a Mander's correlation coefficient (Rr; Fig. 7 D). The data showed an Rr = 0.44 ± 0.041 in control RNAi cells, as compared with an Rr = 0.58 ± 0.06 in cortactin RNAi cells and Rr = 0.65 ± 0.034 in cofilin RNAi cells. Because Rr = 1 indicates complete colocalization, whereas Rr = 0 indicates random colocalization, and Mander's score roughly correlates with percentage of overlap, the data indicated that ∼20%

and Arp2 RNAi cells were quantified and plotted as a function of time as shown in the figure. Initial postactivation values were normalized to 100%. Data represent mean ± AvDev of 32 (control RNAi), 21 (cortactin RNAi), 24 (cofilin RNAi), and 14 (Arp2) single cell time-lapse experiments.

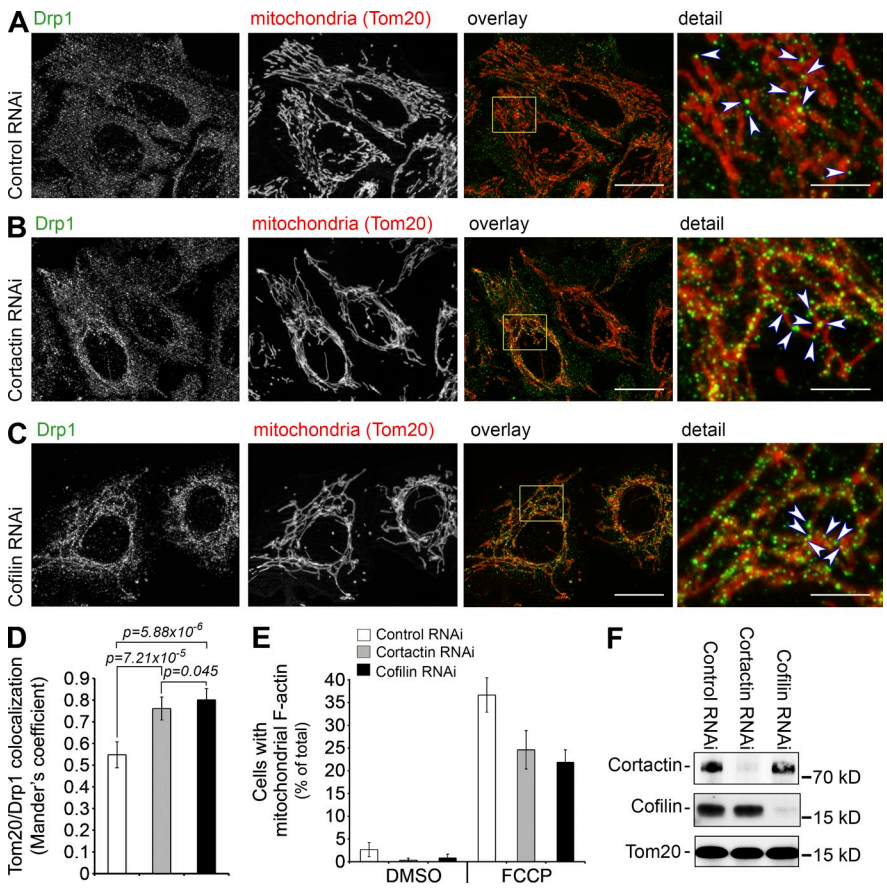


Figure 7. **Mitochondrial accumulation of Drp1 in cortactin and cofilin RNAi cells.** (A–C) Control RNAi (A), cortactin RNAi (B), and cofilin RNAi (C) cells were immunostained for Drp1 (green on overlay and detail images) and Tom20 for mitochondria (red on overlay and detail images). Images were acquired using structured illumination imaging. Maximum projections of seven z-sections acquired at 0.25-µm intervals starting from the bottom of the cell are shown. Bars: 20 µm; (detail) 5 µm. (D) Colocalization of Drp1 with mitochondria was analyzed in control RNAi, cortactin RNAi, and cofilin RNAi cells. The values represent Mander's correlation coefficient (Rr) that reveals the degree of association of pixels in different channels of the image. Data represent the mean ± SD of 15 images/condition. Each image used for the analysis contained at least two cells. (E) Effects of cortactin or cofilin RNAi on accumulation of mitochondrial F-actin in untreated and FCCP-treated (2 min treatment) control RNAi, cortactin RNAi, and cofilin RNAi cells. Data represent mean ± AvDev from a representative experiment after triplicate counting of 150 cells/condition. (F) Cortactin and cofilin protein levels in cells described above (A–E) were analyzed by Western blotting in total cell lysates. Tom20 was used as a loading control.

more of total Drp1 colocalized with mitochondria in cortactin or cofilin RNAi cells than in control RNAi cells. Furthermore, a careful examination of images revealed that submitochondrial Drp1 complexes in cortactin and cofilin RNAi cells were larger than those detected in control RNAi cells (Fig. 7, A–C, arrows).

We also tested the degree to which cortactin and cofilin could regulate stress-induced mitochondrial accumulation of F-actin. Cells were treated with FCCP for 2 min, fixed, and then labeled with Alexa-phalloidin and anti–cytochrome *c* antibody. Quantification revealed that in both cortactin and cofilin RNAi cells (Fig. 7 F), FCCP treatment resulted in reduced numbers of cells displaying mitochondria-associated F-actin compared with control RNAi cells (25.66 ± 4.22 in cortactin RNAi cells and 23.00 ± 2.66 in cofilin RNAi cells compared with 36.67 ± 3.77 in control RNAi cells; Fig. 7 E).

## Mitochondrial association of cortactin, cofilin, and Arp2/3 complexes

Published reports indicate that cortactin, cofilin, and Arp2/3 protein complexes are ubiquitous proteins distributed in the nucleus, cytosol, and membrane compartments of the cell, including the cell membrane, ER, and Golgi complex (Nishida et al., 1987; Yonezawa et al., 1987; Wu and Montone, 1998; Kaksonen et al., 2000; Okreglak and Drubin, 2007). Using structured illumination imaging, we analyzed the spatial relationship between endogenous cortactin, cofilin, or Arp3 and mitochondria in control and FCCP-treated wild-type and Drp1$^{-/-}$ MEFs (Fig. 8). Consistent with published data, in wild-type MEFs cortactin (Fig. 8 A), cofilin (Fig. 8 B), and Arp3 (Fig. 8 C) were abundant within the cytosolic boundaries of the cell without showing strong mitochondria colocalization patterns. However subsets of these proteins colocalized with or were found in close association with mitochondria (Fig. 8, A–C, detail images). Similar localization of ARC/p34, another component of the Arp2/3 complex, was also detected (unpublished data). Although these data do not prove that cortactin, cofilin, and Arp2/3 complexes act at the OMM, we believe that the mitochondrial localization of these proteins, in combination with the data shown in earlier sections of this work, provides evidence suggesting direct mitochondrial roles for cortactin, cofilin, and Arp2/3 complexes. Further supporting this notion, additional mitochondrial accumulation of these proteins was apparent in Drp1$^{-/-}$ MEFs (Fig. 8, D–F). Notably, in many of Drp1$^{-/-}$ cells a mitochondrial pattern of cofilin (Fig. 8 E), Arp3 (Fig. 8 F), and to a lesser degree cortactin (Fig. 8 D) was detectable. Quantitative colocalization analysis also revealed significant increases in the degree of cortactin, cofilin, and Arp3 colocalization with mitochondrial markers in Drp1$^{-/-}$ MEFs, as compared with wild-type MEFs (Fig. 8 G). Although Mander's coefficient (Rr) values in wild-type MEFs were relatively low, in Drp1$^{-/-}$ MEFs they approached values detected for Drp1 colocalization with the mitochondria in wild-type MEFs (see Fig. 1 F). Thus, we conclude that Drp1 knockout leads to robust mitochondrial accumulation of cortactin, cofilin, and Arp3.

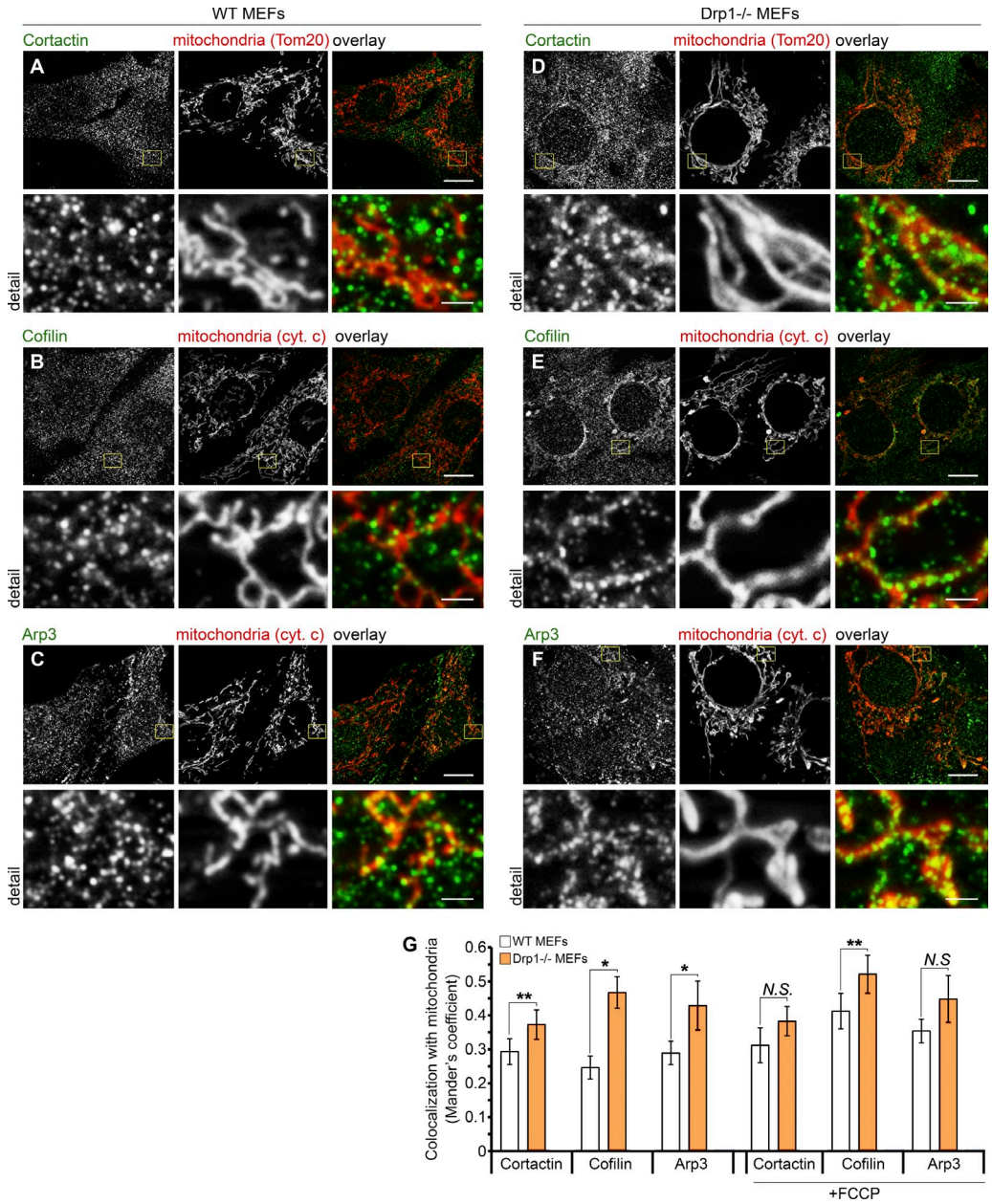


Figure 8. **Mitochondrial association of cortactin, cofilin, and Arp2/3 complexes.** (A–F) Wild-type MEFs (A–C) and Drp1$^{-/-}$ MEFs (D–F) were immunostained with cortactin mAb (A and D; green on overlay images), cofilin (B and E; green on overlay images), and Arp3 (C and F; green on overlay images) polyclonal antibodies, and Tom20 (A and D; red on overlay images) or cytochrome *c* (B, C, E, and F; red on overlay image) to reveal mitochondria. Images were acquired using structured illumination imaging. Single z-sections acquired at 0.25 µm intervals starting from the bottom of the cell are shown. Bars: 20 µm; (detail) 2.5 µm. (G) Colocalization of cortactin, cofilin, and Arp3 with mitochondria in untreated cells and cells treated with FCCP for 2 min were analyzed in wild-type MEFs and Drp1$^{-/-}$ MEFs. The values represent Mander's correlation coefficient (Rr) that reveal the degree of association of pixels in different channels of the image. Data represent the mean ± AvDev of 15 images/condition. Each image used for the analyses contained at least two cells. Statistical significance was determined using a two-tailed *t* test. *, $P < 0.001$; **, $P < 0.01$; N.S., $P > 0.01$.

## Discussion

Here, we show that transient assembly of F-actin on the OMM is vital for the control of Drp1-mediated mitochondrial division. Our data also indicate that F-actin participates in both stress-induced and physiological mitochondrial fission.

It has been proposed that the linear F-actin mediator INF2, and likely linear F-actin fibers, are important for Drp1-dependent mitochondrial fission (Korobova et al., 2013). We found that down-regulation of branched F-actin chain modifying proteins (Kaksonen et al., 2000; Oser et al., 2009; Mooren et al., 2012; Chen and Pollard, 2013; Blanchoin et al., 2014) led to mitochondrial elongation and interconnection, suggesting that cortactin, cofilin, and Arp2/3 complexes, branched F-actin modifying proteins, are also required for mitochondrial fission. However, INF2- and cortactin/cofilin/Arp2/3-dependent regulation of mitochondria is likely to occur through different mechanisms and affect different steps in Drp1-dependent mitochondrial fission. We found that overexpression of ER-localizing INF2 (Chhabra et al., 2009) and dominant active INF2 mutant

(INF2$^{A149D}$) led to actin accumulation on the ER. Furthermore, INF2$^{A149D}$ induced abnormal bundling of F-actin, associated with altered morphology of the ER, as previously shown for the INF2 DAD/WH2 domain mutant (Chhabra et al., 2009). Also as reported previously (Korobova et al., 2013), mitochondrial fragmentation was apparent in INF2$^{A149D}$-expressing cells (unpublished data). However, we were not able to detect transient assembly of F-actin on the mitochondrial fission sites and effects of INF2 and INF2$^{A149D}$ on mitochondrial assembly of Drp1 (unpublished data). Thus, INF2-induced mitochondrial assembly of F-actin might be very transient and not detectable by our imaging setup. Alternatively, based on the fact that overexpression of either INF2 or INF2$^{A149D}$ induces robust F-actin assembly on the ER (unpublished data) and fragmented mitochondria in INF2$^{A149D}$-expressing cells tend to accumulate along an INF2-positive subset of the ER (unpublished data), it is likely that specifically the ER components of the mitochondrial fission pathway are critical for INF2-mediated mitochondrial fission. Under this scenario, INF2 could regulate linear F-actin assembly on the ER tubules that would subsequently redistribute to the mitochondrial fission sites to complete the mitochondrial fission process in a manner reported previously (Friedman et al., 2011). Although we were not able to determine the effect of INF2$^{A149D}$ on mitochondrial assembly of F-actin in an unbiased manner as a result of extensive bundling of F-actin filaments, INF2 overexpression in HeLa did not appear to affect FCCP-induced mitochondrial assembly of F-actin (unpublished data).

We show that down-regulation of the branched F-actin modifying proteins, cortactin and cofilin, led to abnormal accumulation of Drp1 on the mitochondria. Because mitochondrial accumulation of Drp1 is often associated with mitochondrial fragmentation (Frank et al., 2001; Benard and Karbowski, 2009; Braschi et al., 2009; Stavru et al., 2013), Drp1 accumulation on highly interconnected/elongated mitochondria is somewhat counterintuitive. However, it has been shown that overexpression of MiD49/51, mitochondrial receptors of Drp1, or expression of a dominant-negative mutant of MARCH5, a mitochondria-associated E3 ubiquitin ligase, led to mitochondrial accumulation of Drp1 fission complexes associated with abnormal elongation of mitochondria (Karbowski et al., 2007; Palmer et al., 2011; Losón et al., 2013). It is possible that mitochondrial accumulation of Drp1 observed in cortactin or cofilin RNAi cells is a result of inhibition of plausible Drp1 assembly-independent steps of mitochondrial division. Under this scenario, both mitochondrial assembly of Drp1 fission complexes and F-actin–dependent OMM alterations would be required for completion of Drp1-dependent mitochondrial fission. Inhibition of either of these pathways would prevent completion of the other pathway. Indeed, Drp1 accumulated on the mitochondria in cortactin- or cofilin-depleted cells (Fig. 7), whereas F-actin and actin regulatory proteins cortactin, cofilin, and Arp3 accumulated in Drp1-depleted cells (Fig. 8). Similarly, in dynamin1/2$^{-/-}$ double knockout cells, abnormal accumulation of F-actin at endocytic vesicle formation sites was observed (Ferguson et al., 2009), suggesting that F-actin accumulation may point to a similar mechanism in Drp1-depleted cells.

Greater understanding of the molecular mechanism that coordinates mitochondrial assembly of F-actin with Drp1-dependent events of mitochondrial fission is critical. We are currently investigating the potential mitochondrial components that might be implicated in coordination of F-actin and Drp1-dependent steps in mitochondrial fission. One possibility is that MiD49/51 or other mitochondrial receptors of Drp1 could serve this purpose. Supporting this notion, it has been shown that overexpression of MiD49/51 led to inhibition of mitochondrial division associated with both mitochondrial accumulation of inactive Drp1 and abnormal mitochondrial assembly of F-actin (Palmer et al., 2011).

Although the connection between cortactin, cofilin, Arp2/3 complexes, and F-actin assembly on the mitochondria with Drp1-mediated mitochondrial division has not been previously demonstrated, a potential role for cofilin in the regulation of mitochondria has been reported. It was shown that cofilin trans-locates to the mitochondria upon activation of stress-induced apoptosis (Chua et al., 2003; Li et al., 2013) or necrosis (Wabnitz et al., 2010). Because Drp1-mediated mitochondrial fragmentation is one of the events universally linked to stress-induced apoptosis (Youle and Karbowski, 2005), it is possible that cofilin, and perhaps cofilin-dependent mitochondrial F-actin remodeling, also participates in apoptotic fragmentation of the mitochondria. The suggested role of mitochondrial assembly of F-actin in apoptosis-related mitochondrial fission is supported by data showing that in cells treated with various apoptosis inducers, β-actin accumulated on the mitochondria (Tang et al., 2006).

Structured illumination imaging revealed that F-actin localized to the OMM without forming specific submitochondrial foci colocalized with Drp1 and mitochondrial division sites. These findings are at odds with recently published data suggesting that F-actin might form submitochondrial foci specifically at sites where mitochondria interact with the ER (Korobova et al., 2013). Our results showed a diffuse localization of F-actin on the OMM. Although these data do not exclude the possibility that mitochondria-associated F-actin specifically participates in ER tubule– and INF2-mediated mitochondrial fission, they suggest a more widespread role for mitochondrial assembly of F-actin in mitochondrial fission and perhaps other aspects of mitochondrial homeostasis. Most of the proteins implicated in mitochondrial fission in mammalian cells—including Drp1 and Drp1 receptors Mff and MiD49/51, as well as a dominant-negative mutant of MARCH5, a mitochondria-associated E3 ubiquitin ligase—localize to submitochondrial foci forming Drp1 fission complexes (Karbowski et al., 2007; Otera et al., 2010; Friedman et al., 2011; Palmer et al., 2011; Losón et al., 2013). The diffuse mitochondrial appearance of F-actin is rather unique, with the exception of Fis1, another mitochondrial receptor of Drp1 (James et al., 2003; Yoon et al., 2003; Losón et al., 2013). Given the current understanding of how F-actin contributes to membrane scission in non-mitochondrial membrane compartments, it is possible that the OMM assembly and dynamics of F-actin provide mitochondrial division-facilitating alterations of the OMM. Indeed, it has been proposed that in dynamin- and clathrin-dependent endocytosis, local assembly of the F-actin

cytoskeleton led to reorganization of membrane lipids, in particular cholesterol-enriched lipid domains that in turn facilitated vesicle fission (Yao et al., 2013; Dason et al., 2014). It is also likely that F-actin has a critical role in providing a mitochondrial constriction/scission-facilitating force (Skruzny et al., 2012).

## Materials and methods

### Cell culture, transfection, and treatments

HeLa and wild-type, Drp1$^{-/-}$ (Kageyama et al., 2012), Mff$^{-/-}$ (based on the line AZ0438, containing Mff gene trap disruption; Losón et al., 2013), and Mfn2$^{-/-}$ MEFs (Chen et al., 2003) were cultured in DMEM medium supplemented with 10% heat-inactivated fetal bovine serum, 2 mM Glutamax, 1 mM sodium pyruvate, MEM nonessential amino acids (Gibco), 100 U/ml penicillin, and 100 mg/ml streptomycin in 5% $CO_2$ at 37°C. Mfn2$^{-/-}$ and Mff$^{-/-}$ MEFs were provided by D. Chan (Caltech, Pasadena, CA). Cells were transfected with X-tremeGeneHP (Roche) or Lipofectamine2000 (Invitrogen) transfection reagents, according to the manufacturer's instructions. Cells were used for analyses at 16–20 h after transfection. Cell cycle arrest of HeLa cells was performed as previously described (Whitfield et al., 2000). In brief, cells were treated with 2mM thymidine for 18 h, followed by PBS washes and then 9 h in thymidine-free media. Cells were then incubated with 2 mM thymidine for an additional 18 h, followed by washing with PBS. Normal growth medium was added, and then a subset of cells was fixed over time for up to 10 h after the release from the thymidine block. Cell cycle status of the released cells was monitored by flow cytometry after propidium iodide (PI) staining.

### Expression constructs and shRNAi

mRuby-Lifeact construct (Riedl et al., 2008) was provided by T. Blanpied (University of Maryland, Baltimore, MD). mCherry-UtrCH (Burkel et al., 2007) was purchased from Addgene (plasmid 26740; deposited by W. Bement). The Mito-YFP construct was purchased from Takara Bio Inc. GFP-tagged INF2 and INF2 (Korobova et al., 2013) were provided by H. Higgs (Dartmouth Medical School, Hanover, NH). MISSION shRNAi vectors were purchased from Sigma-Aldrich. Cortactin (TRCN0000294181, RNAi#1; TRCN0000294182, RNAi#2; and TRCN0000298256, RNAi#3), cofilin (TRCN0000381606, RNAi#1; TRCN0000381418, RNAi#2; and TRCN0000381720, RNAi#3), gelsolin (TRCN0000343442, RNAi#1; TRCN0000343443, RNAi#2; and TRCN0000352869, RNAi#3), Arp2 (TRCN0000290833), p34 (TRCN0000379644), Opa1 (TRCN0000303506), and Mfn2 (TRCN0000082686) were down-regulated with above-mentioned MISSION shRNAi vectors. eGFP targeting shRNAi construct was used as a control (SHC005). Cells were transfected with respective shRNAi constructs, and then ∼24 h after transfection they were incubated with 3 µg/ml puromycin for an additional 4–5 d to select transfected cells.

### Immunofluorescence

Immunofluorescence was performed as previously described (Benard and Karbowski, 2009; Xu et al., 2011). For immunofluorescence, cells grown in 2-well chamber slides (model 1 German borosilicate; Labtec) were fixed with prewarmed to 37°C 4% PFA in PBS solution for 20 min at RT, and then permeabilized with 0.15% Triton X-100 in PBS for 20 min at RT. After blocking with 7.5% BSA in PBS for 45 min, samples were incubated with primary antibodies in 7.5% BSA in PBS for 90 min at RT, followed by 3 washes with 7.5% BSA in PBS and incubation with secondary antibodies diluted in blocking buffer for 45 min at RT. Samples were washed with PBS at RT, and imaged directly in PBS within 2 d after immunofluorescence processing. The primary antibodies were: anti-Tom20 polyclonal antibody (dilution 1:2,000; clone FL-145; Santa Cruz Biotechnology, Inc.), anti–cytochrome *c* mAb (1:300; clone 6H2.B4; BD), anti-cortactin mAb (1:500; clone 4F11; Millipore), anti-cofilin polyclonal antibody (1:500; clone FL166; Santa Cruz Biotechnology, Inc.), anti-Arp3 polyclonal antibody (1:500; Millipore), anti-ARC/p34 polyclonal antibody (1:500; Millipore), anti-Dlp1 (Drp1) mAb (1:250; clone 8; BD), and anti-Mff polyclonal antibody (1:1,000; ProteinTech). Secondary antibodies were anti–mouse or anti–rabbit Alexa Fluor 488 (1:500; Molecular Probes), or anti–mouse or anti–rabbit Alexa Fluor 546 (1:500; Molecular Probes). F-actin in fixed cells was detected using Alexa 546–phalloidin, according to the manufacturer's protocol (Molecular Probes). In brief, after blocking with 7.5% BSA in PBS, cells were incubated with 6.7 U/ml Alexa 546–phalloidin in blocking buffer for 60 min at RT, washed and then processed for immunofluorescence with respective primary antibodies.

### Image acquisition and analysis

Images were acquired using a fluorescent microscope (AxioObserver Z1; Carl Zeiss), equipped with a 100/1.45 α-Plan-FLUAR objective lens (Carl Zeiss), an ApoTome unit (enabling high-resolution structured illumination image acquisition), a Definitive Focus module, and a CCD camera (QuantEM 512SC; Photometrics) at RT. The ApoTome filters were set to maximum noise elimination. The software used for image acquisition was AxioVision 4.8 (Carl Zeiss). Image cropping and global adjustments to brightness and contrast were performed using Photoshop CS6 software (Adobe).

Live cell imaging was performed using the above-described system. Cells were grown in 2-well chamber slides (model 1 German borosilicate; Labtec) and imaged in Phenol red–free DMEM, supplemented with 10% heat-inactivated fetal bovine serum, 2 mM Glutamax, 1 mM sodium pyruvate, MEM nonessential amino acids, 100 U/ml penicillin, 100 mg/ml streptomycin, and 25 mM Hepes, pH 7.4, at RT.

For colocalization analyses of Drp1 and mitochondria in cortactin and cofilin RNAi cells, seven z-section images (0.25-µm interval between each image), starting from the bottom of the cell (total depth 1.75 µm), were used to make maximum intensity projections using the z-project option of the image analysis software ImageJ (National Institutes of Health). For MEF experiments, single z-sections selected based on the higher amount of mitochondria were used. Colocalization was analyzed using ImageJ plug-in "Mander's Coefficients".

### Mitochondrial fusion assay

Mito-PAGFP–based mitochondrial fusion assay was performed using a confocal microscope (LSM 510 META; Carl Zeiss) equipped with Plan-Apochromat 100×/1.4D oil DIC M27 objective lens (Carl Zeiss) as described previously (Karbowski et al., 2004; Karbowski et al., 2006). In brief, after acquisition of a preactivation image, an ∼5-µm-diameter circular region of interest was photoactivated by brief irradiation with 351/364-nm light (using Coherent Enterprise Ion Laser 80.0mW), followed by time-lapse imaging using 488-nm excitation light and 488-nm Argon Ion Laser (25.0 mW set at 0.3%). 15 postactivation images were collected with interval between images set to ∼2 min. To avoid z-section shift, focus was maintained using the "Multi-time Macro" and the autofocusing system (utilizing linescans to detect the reflection off the coverglass). Images were acquired and analyzed using ZEN 2009 image acquisition software (Carl Zeiss).

### Western blot

Cells were harvested, and total cell protein lysates were prepared as previously described (Xu et al., 2011). In brief, cells were collected, washed with ice-cold PBS, resuspended in SDS PAGE sample buffer, and incubated at 100°C for 10 min. Protein concentrations were measured directly in the samples using NanoDrop 1000 spectrophotometer (Thermo Fisher Scientific). Proteins were separated on 4–20% gradient Tris-Glycine polyacrylamide gels (Invitrogen), transferred onto PVDF membranes (Immubilon-P; Millipore), and incubated with primary antibodies, followed by HRP-conjugated anti–mouse (Roche) or anti–rabbit (Roche) secondary antibodies. Blots were detected with ECL PLUS reagent (GE Healthcare) using ImageQuant LAS4000 chemiluminescence imager (GE Healthcare). Antibodies used for Western blot were: anti-cortactin mAb (clone 4F11; Millipore), anti-cofilin polyclonal antibody (clone FL-166; Santa Cruz Biotechnology, Inc.), anti-Arp2 polyclonal antibody (clone H-84; Santa Cruz Biotechnology, Inc.), anti-ARC/p34 polyclonal antibody (Millipore), anti-Tom20 polyclonal antibody (clone FL-145; Santa Cruz Biotechnology, Inc.), anti-Opa1 mAb (clone 18; BD), and anti-Mfn2 mAb (Abcam).

### Online supplemental material

Fig. S1 presents the submitochondrial distribution of F-actin in FCCP- and Antimycin A–treated cells. Fig. S2 shows spatial relation of F-actin and mitochondria in FCCP-treated Drp1$^{-/-}$ MEFs. Fig. S3 demonstrates typical mitochondrial phenotypes and effect of LatB on the mitochondrial morphology. Fig. S4 shows mitochondrial assembly of F-actin of mRuby-Lifeact in FCCP-treated Drp1$^{K38A}$-expressing living HeLa cells. Fig. S5 shows mitochondrial assembly of mCherry-UtrCH in FCCP-treated living HeLa cells. Online supplemental material is available at http://www.jcb.org/cgi/content/full/jcb.201404050/DC1.

The authors would like to thank Pamela Wright and the members of the Karbowski laboratory for comments on the manuscript, Dr. David Chan for Mfn2$^{-/-}$ and Mff$^{-/-}$ MEFs, Dr. Thomas Blanpied for the mRUBY-Lifeact construct, and Ferenc Livak (Flow Cytometry Core Facility, University of Maryland, Baltimore) for the excellent service provided.

The authors gratefully acknowledge financial support from NIH: R01GM089853 (H. Sesaki), R01 HL105239 and U01 HL116321 (W.J. Lederer), and R01 GM083131 and R01 GM102177 (M. Karbowski).

The authors declare no competing financial interests.

Submitted: 10 April 2014
Accepted: 1 December 2014

## References

Alexander, C., M. Votruba, U.E. Pesch, D.L. Thiselton, S. Mayer, A. Moore, M. Rodriguez, U. Kellner, B. Leo-Kottler, G. Auburger, et al. 2000. OPA1, encoding a dynamin-related GTPase, is mutated in autosomal dominant optic atrophy linked to chromosome 3q28. *Nat. Genet.* 26:211–215. http://dx.doi.org/10.1038/79944

Beck, H., K. Flynn, K.S. Lindenberg, H. Schwarz, F. Bradke, S. Di Giovanni, and B. Knöll. 2012. Serum Response Factor (SRF)-cofilin-actin signaling axis modulates mitochondrial dynamics. *Proc. Natl. Acad. Sci. USA*. 109:E2523–E2532. http://dx.doi.org/10.1073/pnas.1208141109

Benard, G., and M. Karbowski. 2009. Mitochondrial fusion and division: Regulation and role in cell viability. *Semin. Cell Dev. Biol.* 20:365–374. http://dx.doi.org/10.1016/j.semcdb.2008.12.012

Blanchoin, L., R. Boujemaa-Paterski, C. Sykes, and J. Plastino. 2014. Actin dynamics, architecture, and mechanics in cell motility. *Physiol. Rev.* 94:235–263. http://dx.doi.org/10.1152/physrev.00018.2013

Braschi, E., R. Zunino, and H.M. McBride. 2009. MAPL is a new mitochondrial SUMO E3 ligase that regulates mitochondrial fission. *EMBO Rep.* 10:748–754. http://dx.doi.org/10.1038/embor.2009.86

Bravo-Cordero, J.J., M.A. Magalhaes, R.J. Eddy, L. Hodgson, and J. Condeelis. 2013. Functions of cofilin in cell locomotion and invasion. *Nat. Rev. Mol. Cell Biol.* 14:405–415. http://dx.doi.org/10.1038/nrm3609

Bui, H.T., and J.M. Shaw. 2013. Dynamin assembly strategies and adaptor proteins in mitochondrial fission. *Curr. Biol.* 23:R891–R899. http://dx.doi.org/10.1016/j.cub.2013.08.040

Burkel, B.M., G. von Dassow, and W.M. Bement. 2007. Versatile fluorescent probes for actin filaments based on the actin-binding domain of utrophin. *Cell Motil. Cytoskeleton*. 64:822–832. http://dx.doi.org/10.1002/cm.20226

Cereghetti, G.M., A. Stangherlin, O. Martins de Brito, C.R. Chang, C. Blackstone, P. Bernardi, and L. Scorrano. 2008. Dephosphorylation by calcineurin regulates translocation of Drp1 to mitochondria. *Proc. Natl. Acad. Sci. USA*. 105:15803–15808. http://dx.doi.org/10.1073/pnas.0808249105

Chen, Q., and T.D. Pollard. 2013. Actin filament severing by cofilin dismantles actin patches and produces mother filaments for new patches. *Curr. Biol.* 23:1154–1162. http://dx.doi.org/10.1016/j.cub.2013.05.005

Chen, H., S.A. Detmer, A.J. Ewald, E.E. Griffin, S.E. Fraser, and D.C. Chan. 2003. Mitofusins Mfn1 and Mfn2 coordinately regulate mitochondrial fusion and are essential for embryonic development. *J. Cell Biol.* 160:189–200. http://dx.doi.org/10.1083/jcb.200211046

Chen, H., J.M. McCaffery, and D.C. Chan. 2007. Mitochondrial fusion protects against neurodegeneration in the cerebellum. *Cell*. 130:548–562. http://dx.doi.org/10.1016/j.cell.2007.06.026

Chhabra, E.S., V. Ramabhadran, S.A. Gerber, and H.N. Higgs. 2009. INF2 is an endoplasmic reticulum-associated formin protein. *J. Cell Sci.* 122:1430–1440. http://dx.doi.org/10.1242/jcs.040691

Chua, B.T., C. Volbracht, K.O. Tan, R. Li, V.C. Yu, and P. Li. 2003. Mitochondrial translocation of cofilin is an early step in apoptosis induction. *Nat. Cell Biol.* 5:1083–1089. http://dx.doi.org/10.1038/ncb1070

Dason, J.S., A.J. Smith, L. Marin, and M.P. Charlton. 2014. Cholesterol and F-actin are required for clustering of recycling synaptic vesicle proteins in the presynaptic plasma membrane. *J. Physiol.* 592:621–633.

De Vos, K.J., V.J. Allan, A.J. Grierson, and M.P. Sheetz. 2005. Mitochondrial function and actin regulate dynamin-related protein 1-dependent mitochondrial fission. *Curr. Biol.* 15:678–683. http://dx.doi.org/10.1016/j.cub.2005.02.064

DuBoff, B., J. Götz, and M.B. Feany. 2012. Tau promotes neurodegeneration via DRP1 mislocalization in vivo. *Neuron*. 75:618–632. http://dx.doi.org/10.1016/j.neuron.2012.06.026

Ferguson, S.M., A. Raimondi, S. Paradise, H. Shen, K. Mesaki, A. Ferguson, O. Destaing, G. Ko, J. Takasaki, O. Cremona, et al. 2009. Coordinated actions of actin and BAR proteins upstream of dynamin at endocytic clathrin-coated pits. *Dev. Cell*. 17:811–822. http://dx.doi.org/10.1016/j.devcel.2009.11.005

Frank, S., B. Gaume, E.S. Bergmann-Leitner, W.W. Leitner, E.G. Robert, F. Catez, C.L. Smith, and R.J. Youle. 2001. The role of dynamin-related protein 1, a mediator of mitochondrial fission, in apoptosis. *Dev. Cell*. 1:515–525. http://dx.doi.org/10.1016/S1534-5807(01)00055-7

Friedman, J.R., L.L. Lackner, M. West, J.R. DiBenedetto, J. Nunnari, and G.K. Voeltz. 2011. ER tubules mark sites of mitochondrial division. *Science*. 334:358–362. http://dx.doi.org/10.1126/science.1207385

Gandre-Babbe, S., and A.M. van der Bliek. 2008. The novel tail-anchored membrane protein Mff controls mitochondrial and peroxisomal fission in mammalian cells. *Mol. Biol. Cell*. 19:2402–2412. http://dx.doi.org/10.1091/mbc.E07-12-1287

Guo, C., K.L. Hildick, J. Luo, L. Dearden, K.A. Wilkinson, and J.M. Henley. 2013. SENP3-mediated deSUMOylation of dynamin-related protein 1 promotes cell death following ischaemia. *EMBO J.* 32:1514–1528. http://dx.doi.org/10.1038/emboj.2013.65

Ingerman, E., E.M. Perkins, M. Marino, J.A. Mears, J.M. McCaffery, J.E. Hinshaw, and J. Nunnari. 2005. Dnm1 forms spirals that are structurally tailored to fit mitochondria. *J. Cell Biol.* 170:1021–1027. http://dx.doi.org/10.1083/jcb.200506078

James, D.I., P.A. Parone, Y. Mattenberger, and J.C. Martinou. 2003. hFis1, a novel component of the mammalian mitochondrial fission machinery. *J. Biol. Chem.* 278:36373–36379. http://dx.doi.org/10.1074/jbc.M303758200

Kageyama, Y., Z. Zhang, R. Roda, M. Fukaya, J. Wakabayashi, N. Wakabayashi, T.W. Kensler, P.H. Reddy, M. Iijima, and H. Sesaki. 2012. Mitochondrial division ensures the survival of postmitotic neurons by suppressing oxidative damage. *J. Cell Biol.* 197:535–551. http://dx.doi.org/10.1083/jcb.201110034

Kaksonen, M., H.B. Peng, and H. Rauvala. 2000. Association of cortactin with dynamic actin in lamellipodia and on endosomal vesicles. *J. Cell Sci.* 113:4421–4426.

Karbowski, M., D. Arnoult, H. Chen, D.C. Chan, C.L. Smith, and R.J. Youle. 2004. Quantitation of mitochondrial dynamics by photolabeling of individual organelles shows that mitochondrial fusion is blocked during the Bax activation phase of apoptosis. *J. Cell Biol.* 164:493–499. http://dx.doi.org/10.1083/jcb.200309082

Karbowski, M., K.L. Norris, M.M. Cleland, S.Y. Jeong, and R.J. Youle. 2006. Role of Bax and Bak in mitochondrial morphogenesis. *Nature*. 443:658–662. http://dx.doi.org/10.1038/nature05111

Karbowski, M., A. Neutzner, and R.J. Youle. 2007. The mitochondrial E3 ubiquitin ligase MARCH5 is required for Drp1 dependent mitochondrial division. *J. Cell Biol.* 178:71–84. http://dx.doi.org/10.1083/jcb.200611064

Kashatus, D.F., K.H. Lim, D.C. Brady, N.L. Pershing, A.D. Cox, and C.M. Counter. 2011. RALA and RALBP1 regulate mitochondrial fission at mitosis. *Nat. Cell Biol.* 13:1108–1115. http://dx.doi.org/10.1038/ncb2310

Knott, A.B., G. Perkins, R. Schwarzenbacher, and E. Bossy-Wetzel. 2008. Mitochondrial fragmentation in neurodegeneration. *Nat. Rev. Neurosci.* 9:505–518. http://dx.doi.org/10.1038/nrn2417

Korobova, F., V. Ramabhadran, and H.N. Higgs. 2013. An actin-dependent step in mitochondrial fission mediated by the ER-associated formin INF2. *Science*. 339:464–467. http://dx.doi.org/10.1126/science.1228360

Li, G.B., Q. Cheng, L. Liu, T. Zhou, C.Y. Shan, X.Y. Hu, J. Zhou, E.H. Liu, P. Li, and N. Gao. 2013. Mitochondrial translocation of cofilin is required for allyl isothiocyanate-mediated cell death via ROCK1/PTEN/PI3K signaling pathway. *Cell Commun. Signal.* 11:50. http://dx.doi.org/10.1186/1478-811X-11-50

Losón, O.C., Z. Song, H. Chen, and D.C. Chan. 2013. Fis1, Mff, MiD49, and MiD51 mediate Drp1 recruitment in mitochondrial fission. *Mol. Biol. Cell*. 24:659–667. http://dx.doi.org/10.1091/mbc.E12-10-0721

Mooren, O.L., B.J. Galletta, and J.A. Cooper. 2012. Roles for actin assembly in endocytosis. *Annu. Rev. Biochem.* 81:661–686. http://dx.doi.org/10.1146/annurev-biochem-060910-094416

Nishida, E., K. Iida, N. Yonezawa, S. Koyasu, I. Yahara, and H. Sakai. 1987. Cofilin is a component of intranuclear and cytoplasmic actin rods induced in cultured cells. *Proc. Natl. Acad. Sci. USA*. 84:5262–5266. http://dx.doi.org/10.1073/pnas.84.15.5262

Nunnari, J., and A. Suomalainen. 2012. Mitochondria: in sickness and in health. *Cell*. 148:1145–1159. http://dx.doi.org/10.1016/j.cell.2012.02.035

Okreglak, V., and D.G. Drubin. 2007. Cofilin recruitment and function during actin-mediated endocytosis dictated by actin nucleotide state. *J. Cell Biol.* 178:1251–1264. http://dx.doi.org/10.1083/jcb.200703092

Oser, M., H. Yamaguchi, C.C. Mader, J.J. Bravo-Cordero, M. Arias, X. Chen, V. Desmarais, J. van Rheenen, A.J. Koleske, and J. Condeelis. 2009. Cortactin regulates cofilin and N-WASp activities to control the stages of invadopodium assembly and maturation. *J. Cell Biol.* 186:571–587. http://dx.doi.org/10.1083/jcb.200812176

Otera, H., C. Wang, M.M. Cleland, K. Setoguchi, S. Yokota, R.J. Youle, and K. Mihara. 2010. Mff is an essential factor for mitochondrial recruitment of Drp1 during mitochondrial fission in mammalian cells. *J. Cell Biol.* 191:1141–1158. http://dx.doi.org/10.1083/jcb.201007152

Palmer, C.S., L.D. Osellame, D. Laine, O.S. Koutsopoulos, A.E. Frazier, and M.T. Ryan. 2011. MiD49 and MiD51, new components of the

mitochondrial fission machinery. *EMBO Rep.* 12:565–573. http://dx.doi.org/10.1038/embor.2011.54

Riedl, J., A.H. Crevenna, K. Kessenbrock, J.H. Yu, D. Neukirchen, M. Bista, F. Bradke, D. Jenne, T.A. Holak, Z. Werb, et al. 2008. Lifeact: a versatile marker to visualize F-actin. *Nat. Methods*. 5:605–607. http://dx.doi.org/10.1038/nmeth.1220

Riedl, J., K.C. Flynn, A. Raducanu, F. Gärtner, G. Beck, M. Bösl, F. Bradke, S. Massberg, A. Aszodi, M. Sixt, and R. Wedlich-Söldner. 2010. Lifeact mice for studying F-actin dynamics. *Nat. Methods*. 7:168–169. http://dx.doi.org/10.1038/nmeth0310-168

Salbreux, G., G. Charras, and E. Paluch. 2012. Actin cortex mechanics and cellular morphogenesis. *Trends Cell Biol.* 22:536–545. http://dx.doi.org/10.1016/j.tcb.2012.07.001

Skruzny, M., T. Brach, R. Ciuffa, S. Rybina, M. Wachsmuth, and M. Kaksonen. 2012. Molecular basis for coupling the plasma membrane to the actin cytoskeleton during clathrin-mediated endocytosis. *Proc. Natl. Acad. Sci. USA*. 109:E2533–E2542. http://dx.doi.org/10.1073/pnas.1207011109

Stavru, F., A.E. Palmer, C. Wang, R.J. Youle, and P. Cossart. 2013. Atypical mitochondrial fission upon bacterial infection. *Proc. Natl. Acad. Sci. USA*. 110:16003–16008. http://dx.doi.org/10.1073/pnas.1315784110

Stoeber, M., I.K. Stoeck, C. Hänni, C.K. Bleck, G. Balistreri, and A. Helenius. 2012. Oligomers of the ATPase EHD2 confine caveolae to the plasma membrane through association with actin. *EMBO J.* 31:2350–2364. http://dx.doi.org/10.1038/emboj.2012.98

Taguchi, N., N. Ishihara, A. Jofuku, T. Oka, and K. Mihara. 2007. Mitotic phosphorylation of dynamin-related GTPase Drp1 participates in mitochondrial fission. *J. Biol. Chem.* 282:11521–11529. http://dx.doi.org/10.1074/jbc.M607279200

Tang, H.L., A.H. Le, and H.L. Lung. 2006. The increase in mitochondrial association with actin precedes Bax translocation in apoptosis. *Biochem. J.* 396:1–5. http://dx.doi.org/10.1042/BJ20060241

Taylor, M.J., D. Perrais, and C.J. Merrifield. 2011. A high precision survey of the molecular dynamics of mammalian clathrin-mediated endocytosis. *PLoS Biol.* 9:e1000604. http://dx.doi.org/10.1371/journal.pbio.1000604

Tondera, D., S. Grandemange, A. Jourdain, M. Karbowski, Y. Mattenberger, S. Herzig, S. Da Cruz, P. Clerc, I. Raschke, C. Merkwirth, et al. 2009. SLP-2 is required for stress-induced mitochondrial hyperfusion. *EMBO J.* 28:1589–1600. http://dx.doi.org/10.1038/emboj.2009.89

Wabnitz, G.H., C. Goursot, B. Jahraus, H. Kirchgessner, A. Hellwig, M. Klemke, M.H. Konstandin, and Y. Samstag. 2010. Mitochondrial translocation of oxidized cofilin induces caspase-independent necrotic-like programmed cell death of T cells. *Cell Death Dis.* 1:e58. http://dx.doi.org/10.1038/cddis.2010.36

Whitfield, M.L., L.X. Zheng, A. Baldwin, T. Ohta, M.M. Hurt, and W.F. Marzluff. 2000. Stem-loop binding protein, the protein that binds the 3′ end of histone mRNA, is cell cycle regulated by both translational and posttranslational mechanisms. *Mol. Cell. Biol.* 20:4188–4198. http://dx.doi.org/10.1128/MCB.20.12.4188-4198.2000

Wu, H., and K.T. Montone. 1998. Cortactin localization in actin-containing adult and fetal tissues. *J. Histochem. Cytochem.* 46:1189–1191. http://dx.doi.org/10.1177/002215549804601011

Xu, S., G. Peng, Y. Wang, S. Fang, and M. Karbowski. 2011. The AAA-ATPase p97 is essential for outer mitochondrial membrane protein turnover. *Mol. Biol. Cell*. 22:291–300. http://dx.doi.org/10.1091/mbc.E10-09-0748

Yao, L.H., Y. Rao, C. Bang, S. Kurilova, K. Varga, C.Y. Wang, B.D. Weller, W. Cho, J. Cheng, and L.W. Gong. 2013. Actin polymerization does not provide direct mechanical forces for vesicle fission during clathrin-mediated endocytosis. *J. Neurosci.* 33:15793–15798. http://dx.doi.org/10.1523/JNEUROSCI.2171-13.2013

Yonezawa, N., E. Nishida, S. Koyasu, S. Maekawa, Y. Ohta, I. Yahara, and H. Sakai. 1987. Distribution among tissues and intracellular localization of cofilin, a 21kDa actin-binding protein. *Cell Struct. Funct.* 12:443–452. http://dx.doi.org/10.1247/csf.12.443

Yoon, Y., E.W. Krueger, B.J. Oswald, and M.A. McNiven. 2003. The mitochondrial protein hFis1 regulates mitochondrial fission in mammalian cells through an interaction with the dynamin-like protein DLP1. *Mol. Cell. Biol.* 23:5409–5420. http://dx.doi.org/10.1128/MCB.23.15.5409-5420.2003

Youle, R.J., and M. Karbowski. 2005. Mitochondrial fission in apoptosis. *Nat. Rev. Mol. Cell Biol.* 6:657–663. http://dx.doi.org/10.1038/nrm1697

Züchner, S., I.V. Mersiyanova, M. Muglia, N. Bissar-Tadmouri, J. Rochelle, E.L. Dadali, M. Zappia, E. Nelis, A. Patitucci, J. Senderek, et al. 2004. Mutations in the mitochondrial GTPase mitofusin 2 cause Charcot-Marie-Tooth neuropathy type 2A. *Nat. Genet.* 36:449–451. http://dx.doi.org/10.1038/ng1341

Zunino, R., A. Schauss, P. Rippstein, M. Andrade-Navarro, and H.M. McBride. 2007. The SUMO protease SENP5 is required to maintain mitochondrial morphology and function. *J. Cell Sci.* 120:1178–1188. http://dx.doi.org/10.1242/jcs.03418

Zunino, R., E. Braschi, L. Xu, and H.M. McBride. 2009. Translocation of SenP5 from the nucleoli to the mitochondria modulates DRP1-dependent fission during mitosis. *J. Biol. Chem.* 284:17783–17795. http://dx.doi.org/10.1074/jbc.M901902200